SCIENTIFIC Publishing Limited

Digital Technologies Research and Applications
http://ojs.ukscip.com/index.php/dtra

Article

Enhancing Micro-Pump Efficiency: Multi-Objective Optimization of Low Voltage MEMS Switches for Drug Delivery Applications

Alireza Ardehshiri [1], Farzad Soltanian [1,2,*], Masoud Moradkhani [1] and Mehdi Nosrati [3]

[1] Department of Electrical Engineering, Ilam branch, Islamic Azad University, Ilam 6931133145, Iran
[2] Department of Electrical and Computer engineering, University of Alberta, Edmonton AB T6G 2M9, Canada
[3] Department of Electrical Engineering, Manhattan College, New York NY 10471, USA
[*] Correspondence: fa.soltanian@iau.ac.ir

Received: 17 January 2024; **Revised:** 26 April 2024; **Accepted**: 21 May 2024; **Published**: 30 May 2024

Abstract: This paper introduces an innovative approach for designing, optimizing, and simulating a low voltage MEMS switch specialized for micro-pump applications. The primary goal is to improve the efficiency of micro-pumps used in drug delivery. The design process focuses on tailoring the switch's geometry for micro-pump purposes and employs objective functions encompassing actuation voltage, insertion loss in the up-state, and isolation in the down-state. To solve the intricate optimization task, mathematical programming is combined with the Multi-Objective Particle Swarm Optimization (MOPSO) meta-heuristic algorithm, enabling simultaneous consideration of actuation voltage, insertion loss, and isolation. By analyzing the Pareto front derived from these parameters, the study identifies design requirements and optimal levels for the switch. The proposed MEMS switch demonstrates remarkable performance metrics, including S_{11} and S_{21} values of –11.74 dB and –34.62 dB at 40 GHz, a pull-in voltage of 2.8 V, and an axial residual stress of 25 MPa. This research presents an innovative strategy for optimizing capacitive switch MEMS models, using a multi-objective approach and the MOPSO algorithm to enhance efficiency in micro-pump applications.

Keywords: switch MEMS; Multi-Objective Particle Swarm Optimization (MOPSO) algorithm; uti-liti algorithm; spring constant; actuation voltage

1. Introduction

Bio-electromechanical micro-systems (Bio-MEMS) use micro-sized components, such as sensors, transducers, mechanical actuators, and electronic equipment. Bio-MEMS refers to any type of MEMS used in biological applications. As an example, micropumps can be used, which is an electromechanical system used for advanced drug delivery. Various actuation mechanisms, including electrostatics, piezoelectricity, thermo-pneumatics, bimetallic electro-thermal expansion, shape-memory effects, or ionic conductive polymer films, are necessary for operating mechanical micropumps. One of the challenges of making micro pumps is making a membrane on the pump, which is known as a switch pump [1].

Micro Electromechanical Systems (MEMS) represent a technological process capable of integrating intricate systems and components comprising both electrical and mechanical elements [2]. In reference [3], a method for fault detection and diagnosis of RF MEMS resonators on transceiver boards was proposed, utilizing Lyapunov theory and neural networks to ensure continuous operation by identifying and compensating for fatigue-related faults. MEMS switches are widely acknowledged for their efficiency in applications such as fuzzy array systems and switching filters for wireless communication, owing to their low power consumption, high isolation, minimal insertion loss (typically around 0 dB up to 100 GHz for RF MEMS switches), and superior linear performance

compared to diodes or FET switches [4]. Nevertheless, MEMS switches exhibit weaknesses in terms of high actuation voltage and switching time.

Various stimulating mechanisms, including electrostatic, electromagnetic, piezoelectric, or thermal designs, can be employed to establish two crucial types of MEMS switches: ohmic (serial switches) and capacitive (shunt switches). These switches can operate on microstrip lines and coplanar waveguide (CPW) lines on substrates such as glass, silicon, and GaAs, supporting configurations up to 100 GHz frequencies. When no voltage is applied to the suspended bridge, the central conductor transmits the signal and generates an electrostatic force upon applying an electrical signal to the suspended bridge. Consequently, the conductor lowers the suspended bridge, grounds the central conductor, and blocks signal passage. A dielectric layer is typically incorporated on the CPW transmission line to prevent metal-to-metal contact, corrosion, and metal fatigue due to frequent connections.

Crucial parameters in MEMS switch design include isolation, operating time, electrostatic actuation voltage, stability against temperature variations, and transmission losses [2]. Numerous studies have addressed these parameters: A capacitive switch on a glass sub-layer achieved −35 dB isolation and −0.4 dB insertion loss within a 0 to 20 GHz frequency range [5]. Reference [6] presented a switch with a low spring constant and a 7 V actuation voltage. Additionally, reference [7] reported a switch with a −5.6 dB insertion loss and −24.38 dB isolation at a 40 GHz frequency using a 3.04 V output voltage. Similarly, reference [8] introduced a switch with -0.7 dB insertion loss and −30 dB isolation at 40 GHz frequency with an output voltage of 4.8–6.8 V. Reference [9] demonstrated a switch with −3 dB insertion loss and −13 dB isolation at 40 GHz frequency using an output voltage of 11.7 V. Reference [10] achieved −0.34 dB insertion loss and −72.4 dB isolation at 40 GHz frequency with a 12 V output voltage. Furthermore, reference [11] presented a switch with −0.8 dB insertion loss and −30 dB isolation at 40 GHz frequency using a 25 V output voltage. Finally, reference [12] utilized a 3 V output voltage at 40 GHz frequency, and reference [13] achieved −9 dB insertion loss and −42 dB isolation at 13.5 GHz frequency with a 15–16 V output voltage.

Patients suffering from chronic illnesses necessitate precise drug delivery within short durations. Addressing this imperative, we have devised a mechanism facilitating automated drug administration to patients. Moreover, it is advantageous to engineer a switch characterized by low voltage consumption to mitigate potential adverse effects on the human body. Additionally, a low-voltage switch contributes to the prolonged lifespan of micro pumps. Consequently, we present in this study a Micro Pump Switch MEMS exhibiting superior quality. Furthermore, this innovative structure holds promise for application in transmission lines, exhibiting a significant reduction in insertion loss parameters compared to conventional low-voltage RF MEMS switches.

The current study presents a method for optimizing the multi-objective functions, namely voltage actuation and RF parameters, of a switch through mathematical programming. The developed model is then solved using the MOPSO meta-heuristic algorithm. Furthermore, this model is applied to design a MEMS switch with reduced electrostatic actuation voltage and enhanced insertion loss and isolation, achieved by selecting appropriate structural dimensions (width, length, and thickness) and utilizing the Pareto front obtained for the designed beam spring constant. The paper is structured as follows: Section 2 assesses the performance of the switch. Section 3 delves into the model details and showcases the Pareto front solution set for actuation voltage, insertion loss in the up-state, and isolation in the down-state, obtained by solving the proposed model using MOPSO and the utility algorithm. Section 4 conducts simulations of the target switch and evaluates essential parameters such as actuation voltage, operating time, insertion loss, and isolation. The designed switch is analyzed in Section 5. Finally, Section 6 summarizes the findings and draws conclusions.

2. MEMS Switch Performance

2.1. Micro-Pumps

Micro-pumps are increasingly prominent in biomedical microelectromechanical systems (BioMEMS) devices for measuring small-scale mechanical movements, typically employing silicon-based cantilevers due to their availability and seamless integration with silicon-based technology. Various types of micropumps find application across diverse fields. Below are some commonly encountered types:

(1) Electrostatic Micropumps: These micropumps harness electrostatic forces to generate fluid flow. They typically comprise a flexible diaphragm and electrodes that create pressure differentials to manipulate fluid movement.
(2) Piezoelectric Micropumps: These pumps leverage the piezoelectric effect; wherein specific materials generate an electric charge under mechanical stress. This phenomenon is utilized to induce fluid flow.
(3) Thermal Micropumps: These pumps utilize thermal energy to induce fluid flow, employing mechanisms that capitalize on temperature differentials to drive fluid movement. They often have micromachined structures containing heating elements that cause localized temperature gradients, leading to convective flow [14].

Reference [15] provides an extensive examination of the potential of microfluidic actuators in drug dosing, emphasizing their capacity to reduce size and energy consumption while facilitating innovative therapies. Despite these benefits, the scarcity of industrial micro dosing units indicates limited adoption. The authors delve into the specific challenges within medical dosing, encompassing safety, precision, and system limitations, and scrutinize mechanical micropumps for drug delivery. They survey existing industrial micro dosing systems, underscoring the imperative for further research to optimize pump efficacy, address safety apprehensions, and ensure compatibility with diverse medications. In essence, while micropumps hold significant promise for augmenting drug dosing applications, sustained exploration and refinement are imperative to surmount extant obstacles and encourage widespread acceptance.

Additionally, reference [16] delves into the progression of various micropump technologies over the preceding three decades, recognizing their maturation and established performance benchmarks. It anticipates future healthcare trends, emphasizing enhanced device connectivity through smartphone applications to enrich patient engagement and treatment compliance, alongside the escalating demand for monitoring infusion precision, micropump functionality, and physiological metrics relevant to therapy. Nonetheless, despite the considerable research devoted to micropumps, ancillary components of drug delivery apparatuses, such as drug reservoirs and fluidic connections, have received comparatively less attention. Challenges persist in devising secure, biocompatible, and dependable reservoirs that uphold pumping efficacy over time, as well as ensuring compatibility with sterilization procedures. Furthermore, standardizing microfluidic connections and reservoir platforms to accommodate diverse micropump variants could streamline FDA approval processes and expedite time-to-market for drug delivery apparatuses. Figure 1 illustrates an electrostatic micro-pump is a device used to generate fluid flow on a small scale, typically in microfluidic systems. It operates based on the principles of electrostatic forces. The pump consists of a flexible diaphragm or membrane, typically made of a polymer material, which separates two fluid chambers. Each chamber has electrodes integrated into it, and applying an electric voltage between the electrodes generates electrostatic forces. These forces cause the diaphragm to deform and generate pressure gradients, resulting in fluid movement [17].

The working principle of an electrostatic micro-pump involves two main stages: the compression phase and the relaxation phase. During the compression phase, an electric field is applied, attracting the diaphragm toward one chamber and compressing the fluid [16]. As a result, the fluid is pushed toward the outlet. In the relaxation phase, the electric voltage is switched off, allowing the diaphragm to return to its original position, creating a suction effect and drawing fluid from the inlet. The advantages of electrostatic micro-pumps include their small size, low power consumption, and compatibility with a wide range of fluids. However, they may face challenges related to clogging, limited maximum flow rates, and potential reliability issues associated with diaphragm fatigue. The electrostatic micro-pump membrane is a flexible component within an electrostatic micro-pump that plays a crucial role in generating fluid flow. The membrane of an electrostatic micro-pump is designed to be responsive to electrostatic forces. It deforms when an electric voltage is applied across the electrodes, generating pressure gradients that propel the fluid through the system. The membrane acts as a barrier between the two chambers, preventing fluid mixing while allowing controlled fluid displacement. The design and dimensions of the membrane also contribute to the pump's performance. Factors such as thickness, size, and shape of the membrane influence the generated pressure differentials, flow rates, and response time of the pump. Optimizing these parameters ensures efficient and reliable fluid movement [18].

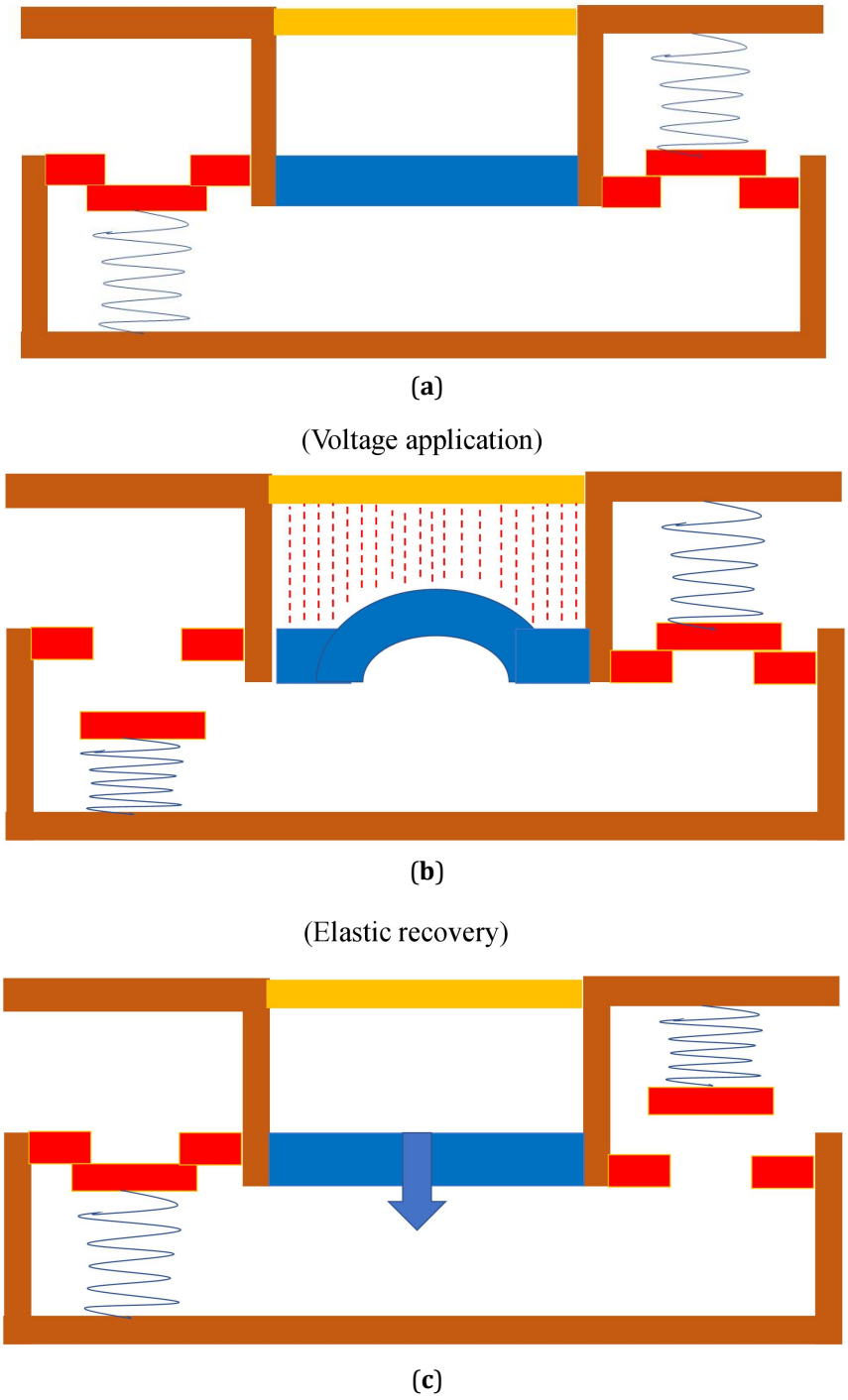

Figure 1. The schematic of the electrostatic micro-pump. (**a**) Normal situation; (**b**) Voltage application; (**c**) Elastic discovery.

2.2. Switch Spring Constant and Excitation Voltage

Figure 2 illustrates a configuration of parallel MEMS switches. In this arrangement, the lower electrode functions as the central transmission line of the waveguide, while the upper electrode consists of a thin metal sheet suspended from the lower electrode and linked to the lateral conductors of the coplanar waveguide. Moreover, a thin dielectric layer covers the lower electrode to prevent direct metal connections [19].

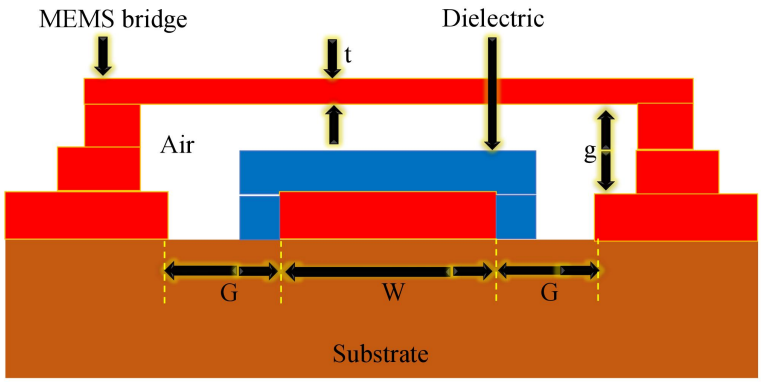

Figure 2. The schematic of the switch.

The switch depicted in Figure 2 can transition between two positions, namely up and down, through the application of a DC actuation voltage. The gap between the electrodes influences the ratio of capacitors in the on and off states, as well as the isolation. When no excitation voltage is present, the upper electrode acts as a minor parasitic capacitor, usually negligible under ideal conditions. The electrostatic actuation voltage for the capacitance switches is determined using Equation (1) [20].

$$V = V\left(\frac{2}{3}g_0\right) = \sqrt{\frac{8k}{27\varepsilon_0 A}{g_0}^3} \tag{1}$$

where ε_0, g_0, and k represent the vacuum permittivity coefficient, the air gap between the suspended bridge and the transmission line at zero electrostatic actuation voltage, and the spring constant of the beam, respectively. Reducing g_0 $(g_0 = g_{gap} + t_{hd})$ and increasing the area of the switch (A) can result in a lower spring constant [21,22]. One effective approach to reduce the actuation voltage is by decreasing the spring constant k, which can be achieved through the design of a more flexible structure. Numerous studies have explored methods to control and diminish the spring constant value [23]. Figure 3 illustrates that applying voltage to the bridge induces a variation in capacitance, i.e., a variable capacitor. The value of the variable capacitor C_u, C_d depends on the voltage applied to the suspended bridge. Furthermore, the capacitance C_u and C_d correspond to the upstate and downstate of the capacitor, respectively, and their values are calculated based on Equations (2) and (3) [20]:

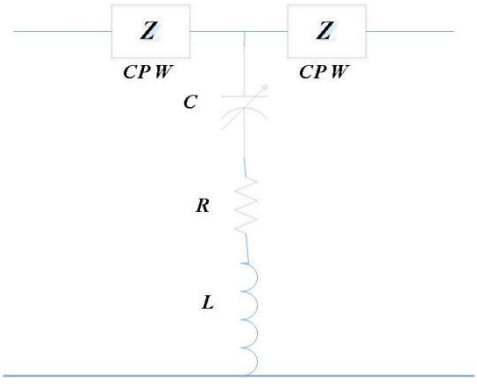

Figure 3. The electric model consists of switch MEMS.

$$C_d = \frac{\varepsilon_0 \varepsilon r\, Ww}{t_d} \tag{2}$$

$$C_u = \frac{\varepsilon_0 Ww}{g_{gap} + (\frac{t_d}{\varepsilon_r})} \tag{3}$$

where W_w denotes the switch area, t_d represents the thickness of the dielectric, and ε_0 denotes vacuum permittivity. The S-parameters are initially measured in the up-state position data (S_{11}) and fitted to obtain the up-state capacitance of the switch (S_{21}). S_{11} and S_{21} are acquired using Equations (4) and (5) [20]:

$$S_{11}(up\ state) = \frac{-j\omega c_u z_0}{2 + j\omega c_u z_0} \Rightarrow \left|{S_{11}}^2\right| = \frac{\omega^2 {Z_0}^2 (\varepsilon_0 W w)^2}{4(g_{gap} + (\frac{t_d}{\varepsilon_r}))^2} \tag{4}$$

$$S_{21}(down\ state) = \frac{2}{2 + j\omega c_p z_0} \Rightarrow \left|{S_{21}}^2\right| = \frac{4{t_d}^2}{\omega^2 {Z_0}^2 (\varepsilon_0 \varepsilon_r W w)^2} \tag{5}$$

where Z_0 represents the impedance of the transmission line, set at 50 Ohms, and ω is the angular frequency.

3. MEMS Switch Design

3.1. Principles for Mathematical Programming

Mathematical programming, a method grounded in problem modeling, utilizes programming techniques to optimize decision-making processes. Operations research methodologies involve observation, definition, modeling, model solving, and model implementation, crucial for yielding research outcomes [24]. In mathematical programming, the formulation of a problem model requires adherence to four key components: the objective function, constraints, decision variables, and parameters [24]. The Pareto front, representing an optimal vector dominating others within the solution space, emerges from the solution set of the objective function [25]. For RF switch MEMS optimization, a multi-objective integer programming model is proposed, aiming to minimize actuation voltage while maximizing insertion loss in the up-state and isolation in the down-state. Table 1 details the objective function, constraints, decision variables, and parameters of this mathematical model.

In the design of the improved switch MEMS outlined herein, we adopt the structure previously proposed in reference [9]. Parameters W and L denote the width and length of the RF Coplanar Waveguide (CPW), set at 80 and 200 micrometers, respectively, following the configuration outlined in reference [9]. Additionally, CPW parameters are aligned with a 50-ohm characteristic impedance. Our analysis focuses on the individual performance of the designed switch MEMS at an operational frequency of 40 GHz, rather than across the entire frequency spectrum.

Table 1. Parameters and Decision variables of this paper mathematical model.

Parameters				
AL Young's modulus (E)	AL Poisson's ratio (v)	Switch thickness (t)	Vacuum permittivity (ε_0)	switch Width (W)
70 GPa	0.32	0.877 μm	8.85×10^{-12} N/A^2	80 μm
Decision Variables				
spring constant (k)	switch Length (W)	Dielectric layer thickness (t_d)	Air gap (g_{gap})	Angular frequency of operation (ω)

3.2. Objective Functions

The objective functions aim to achieve the following goals: Minimization of the actuation voltage, based on Equation (1), Maximization of the insertion loss in the up-state, formulated according to Equation (4), Minimization of the isolation in the down-state, derived from Equation (5), and the mathematical model presented in this paper is encapsulated in Equations (6)–(9).

$$\text{Actuation voltage: } Min:\ Z_1 = V = \sqrt{\frac{8k}{27\varepsilon_0 Ww}{g_0}^3} \tag{6}$$

$$\text{Insertion loss up state: } Max: Z_2 = |S_{11}|^2 = \frac{\omega^2 {Z_0}^2(\varepsilon_0 Ww)^2}{4(g_{gap} + (\frac{t_d}{\varepsilon_r}))^2} \tag{7}$$

$$\text{Isolation down state: } Min: Z_3 = |S_{21}|^2 = \frac{4{t_d}^2}{\omega^2 {Z_0}^2(\varepsilon_0 \varepsilon_r Ww)^2} \tag{8}$$

Subject to:

$$\begin{cases} 1\ \text{N/m} \le k \le 1.4\ \text{N/m} \\ 150\ \mu\text{m} \le W \le 200\ \mu\text{m} \\ 1.1\ \mu\text{m} \le g_{gap} \le 1.4\ \mu\text{m} \\ 10\ \text{GHz} \le \omega/2\pi \le 120\ \text{GHz} \\ 0.085\ \mu\text{m} \le t_d \le 0.11\ \mu\text{m} \end{cases} \tag{9}$$

4. Multi-Objective Particle Swarm Optimization

4.1. (MPSO) Algorithm

Particle swarm algorithm is an evolutionary algorithm for the optimization of nonlinear functions presented based on the social behavior of birds. This algorithm was introduced [26], which was derived from the behavior of invasive particles like the crows [27]. The MOPSO algorithm is solved by the following Equations (10) and (11).

$$V_i(t) = w \times V_i(t-1) + c_1 \times rand1 \times (P_{i.best} - X_i(t_1)) + c_2 \times rand2 \times (P_{g.best} - X_i(t-1)) \tag{10}$$

$$X_i = X_i(t-1) + V_i(t) \tag{11}$$

where the velocity V_{ik} of the i^{th} particle at the iteration k^{th} is determined by the current solution x_{ik} (or position) of the particle at that iteration. c_1 and c_2 are positive constants, while r_1 and r_2 are two random variables with a uniform distribution between 0 and 1. In this equation, w represents the inertia weight, indicating the influence of the previous velocity vector on the new vector. An upper bound is imposed on the velocity in all dimensions V_{max}. This limitation prevents the particle from moving too rapidly from one region in the search space to another. This value is usually initialized as a function of the range of the problem [27]. After tuning the MOPSO parameters, the model RF switch MEMS problem is solved in MATLAB software. The visualization of the estimates of the Pareto front for the case study problem is depicted in Figure 4. In addition, the best values for the algorithm's parameters defined in Table 2.

Table 2. Best parameters for MOPSO algorithm.

Population Size	Number of Iterations	Velocity Limits $\mathbf{Vel_{Max}}$	Inertia Weight Damping Ratio $\mathbf{W_{damp}}$
250	500	0.15	0.98

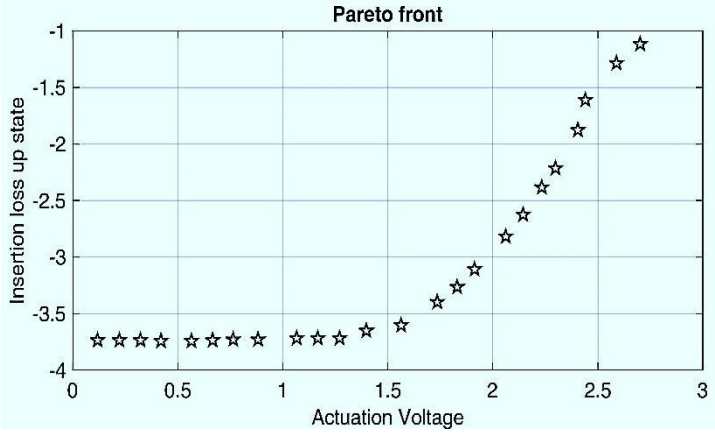

(**a**) Insertion loos (in the up-state situation) verses actuation voltage.

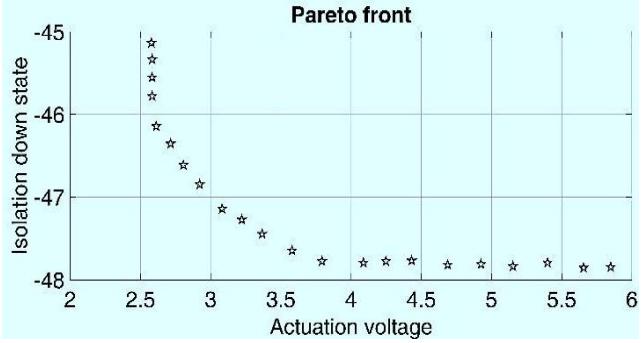

(**b**) Isolation (in the down state situation) verses actuation voltage.

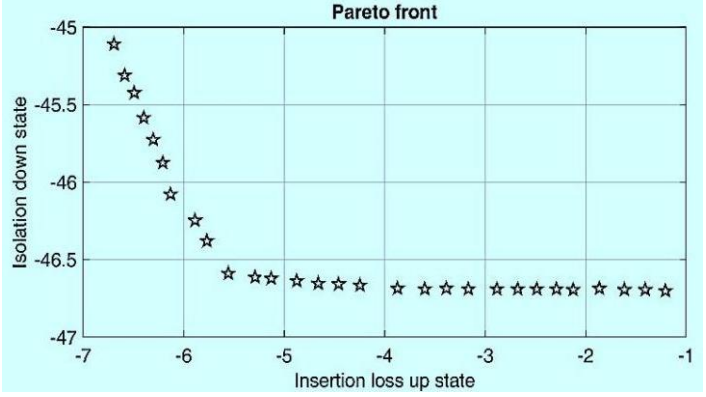

(**c**) Isolation (in the down state situation) verses Insertion loos (in the up-state situation).

Figure 4. The visualization of the estimates of the Pareto front for the case study problem in MATLABE software.

4.2. Uti-liti Algorithm

Each set of solutions represents a scenario for the development of a capacitance switch. With a preference for solutions that align closely with the target values, an approach based on the utility of the target functions was employed to identify the optimal solution. This approach aims to minimize the distance of each target function from its respective best value in the reported answer set, ensuring the utility value Ui is equal to 1 when each target function achieves its best value and 0 when it reaches its worst possible value. Equation (12) is optimized to ensure that the utility related to the target function equals 1. Given Equations (13)–(16) [9], the utility value equals 1 when each target function attains its best value and 0 when it reaches its worst possible value [28].

$$max\ \gamma \tag{12}$$

$$\gamma = min\,(U_1, U_2, U_3) \tag{13}$$

$$U_1 = \left(\frac{Z_1^{max} - Z_1}{Z_1^{max} - Z_1^{min}}\right) \tag{14}$$

$$U_2 = 1 - \left(\frac{Z_2^{max} - Z_2}{Z_2^{max} - Z_2^{min}}\right) \tag{15}$$

$$U_3 = \left(\frac{Z_3^{max} - Z_3}{Z_3^{max} - Z_3^{min}}\right) \tag{16}$$

Table 3 presents the values associated with the best, worst, and final outcomes of the target functions in the selected solution. Following the proposed utility algorithm, the optimal values for the actuation voltage, insertion loss in the up-state, and isolation in the down-state are V = 2.801 V, S_{11} = –11.08 dB, and S_{21} = –46.91 dB, respectively.

Table 3. Final value of the target function.

n	V	S_{11}	S_{21}	U_1	U_2	U_3	γ
1	2.801	–5.493	–47.517	0.988	0.182	0.063	0.063
2	2.837	–5.497	–48.209	0.565	0	0.978	0
3	2.821	–5.487	–46.220	0.765	0.455	0.992	0.455
4	2.802	–5.498	–46.693	0.988	0.091	0.296	0.091
5	2.851	–5.485	–46.224	0.412	0.545	0.997	0.412
6	2.846	–5.475	–46.226	0.471	1	1	0.471
7	2.886	–5.476	–46.225	0	0.955	0.999	0
8	2.861	–5.490	–46.214	0.294	0.318	0.984	0.294
9	2.826	–5.484	–46.222	0.706	0.591	0.995	0.591
10	2.809	–5.495	–46.185	0.894	0.091	0.946	0.091
11	2.801	–5.494	–46.469	1	0.136	0	0
12	2.862	–5.482	–46.224	0.282	0.682	0.997	0.282
13	2.801	–5.493	–46.517	0.988	0.182	0.063	0.063
14	2.837	–5.497	–46.209	0.565	0	0.978	0
15	2.821	–5.487	–46.220	0.765	0.455	0.992	0.455
16	2.802	–5.495	–46.693	0.988	0.091	0.296	0.091
17	2.851	–5.485	–46.224	0.412	0.545	0.997	0.412
18	2.846	–5.475	–46.226	0.471	1	1	0.471

The optimal solution for the switch is identified in row 13 of Table 3. According to the proposed algorithm, the optimal switch design is detailed in Table 4.

Table 4. Optimal switch design.

n	V	S_{11}	S_{21}	U_1	U_2	U_3	γ
9	2.826	−5.484	−46.222	0.706	0.591	0.995	0.591
Variables							
k	w	g_{gap}	$\omega/2\pi$	t_{hd}			
1.033	199.973	1.410	39.969	0.086			

4.3. Switch Spring Constant

The spring constant described in Equation (17) is derived from the design of spiral beams, as depicted in Figure 5 [29]. Table 5 displays the parameters corresponding to Equation (17).

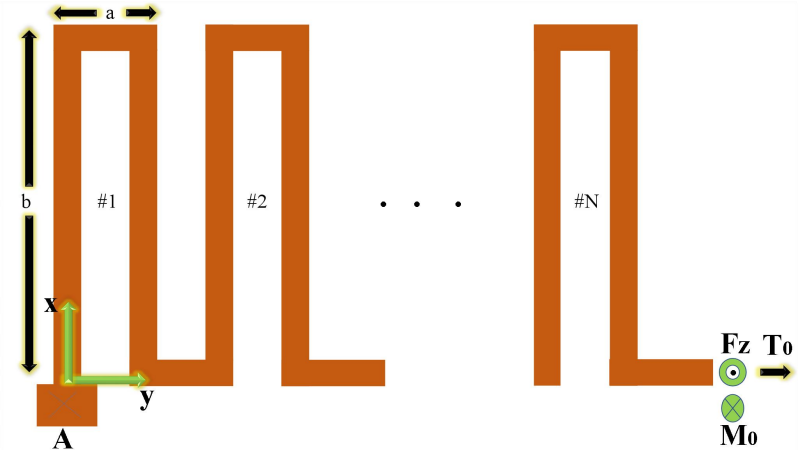

Figure 5. Spiral Beams Design.

$$k_z = \left[\left[\frac{(8N^3a^3)+(2Nb^3)}{3EI_x} + \frac{abN[3b+(2N+1)(4N+1)a]}{3G_j}\right] - \left[\frac{N\,a^2\left[\left(\frac{2Na}{EI_X}\right)+\frac{(2N+1)b}{G_j}\right]^2}{2\left(\frac{a}{EI_X}+\frac{b}{G_j}\right)} - \frac{Nb^2}{2}\left(\frac{a}{G_j}+\frac{b}{EI_X}\right)\right]^{-1}\right] \quad (17)$$

Table 5 presents the parameters of the Equation (17).

Table 5. The 17th equation parameters.

a	b	Shear Module (G)	Polar Moment of Inertia (I_P)	Torsion Constant (J)
4.5μm	45 μm	$E/2(1+v)$	$I_x + I_z$	0.413IP
Beam Width (w_1)		**x-axis Moment of Inertia (I_x)**		**z-axis Moment of Inertia (I_z)**
1.5 μm		$wt^3/12$		$wt^3/12$

5. Designed Switch Analysis

This should clearly explain the main conclusions of the article, highlighting its importance and relevance. This section is not mandatory but can be added to the manuscript if the discussion is unusually long or complex.

5.1. Electro-Mechanic Analysis

The proposed design underwent simulation using COMSOL software. Various boundary conditions were employed in this design, including: Fixing the end of the beam to prevent movement, applying zero voltage to the dielectric subsurface, Applying the bias voltage to the membrane surface, implementing symmetry conditions to reduce computational complexity, utilizing boundary load conditions on the beam subsurface to prevent infinite displacement errors, and applying boundary conditions of the electrical DC voltage on the switch level to mimic real-world operation.

The simulation involves calibrating the element size for general physics, with a range between 1.98 and 11 μm. Parameters such as the maximum element growth rate, curvature factor, and resolution of the narrow factor are set to 1.5, 0.6, and 0.5, respectively. The geometric entity level is designated as boundary, and both the number of iterations and maximum element depth are set to 4. The interpolation method is automatic, and the mesh graphic is illustrated in Figure 6.

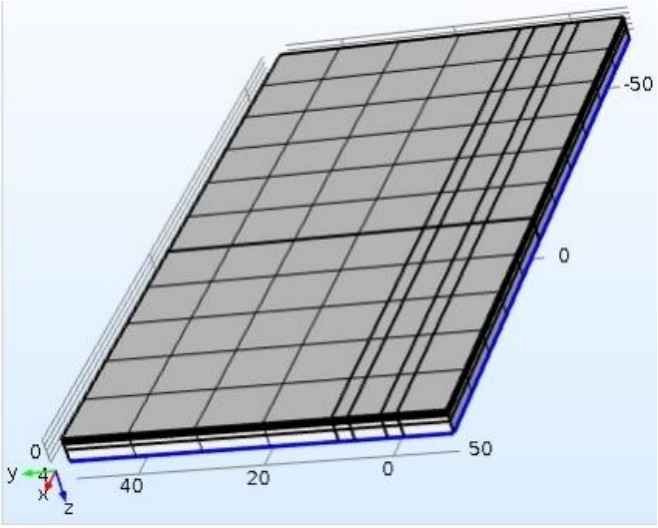

Figure 6. Mesh graph of the proposed model.

Figure 7 depicts the simulation results of the optimized switch design. It is evident that applying an actuation voltage of 2.8 V to the membrane surface induces a displacement of 1.4 μm, effectively reducing the transmission line voltage to zero. Figure 8 illustrate the results the axial residual stress. The axial residual stress resulting from applying the voltage to the switch surface is equal to σ = 25 MPa.

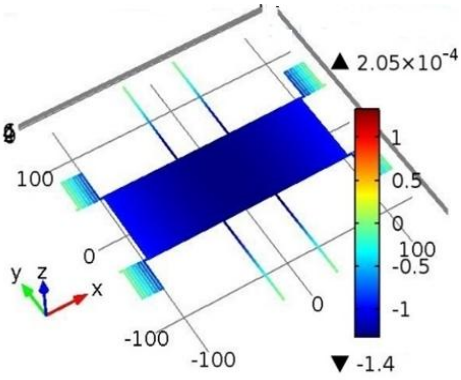

Figure 7. Z-displacement distribution (μm).

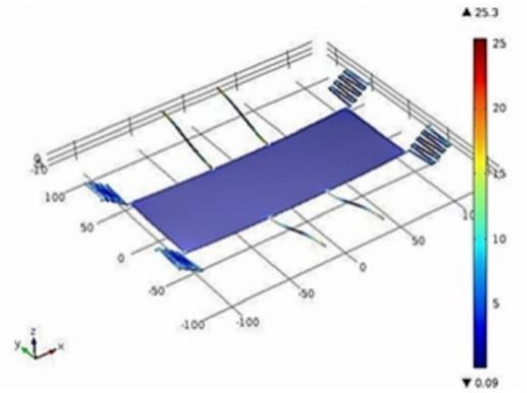

Figure 8. Von Misses stress distribution (MPa).

5.2. Switch Operation Time and Capacitor Variations

The response time of the switch, which relies heavily on the applied voltage to the beam membrane, has been optimized to approximately 15 μs through careful design and the use of electrostatic actuation voltage, as depicted in Figure 9. Additionally, higher actuation voltages can further expedite response times. Consequently, the capacitance reaches approximately 7 pF when the electrostatic actuation voltage is applied to the switch. Upon discontinuation of the electrostatic actuation voltage, the capacitor value decreases to 0.1 pF, as illustrated in Figure 10.

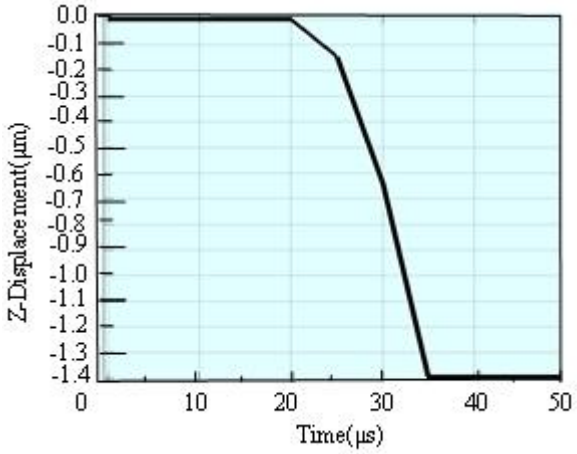

Figure 9. Simulation of the optimized switch in time domain. Membrane's movement.

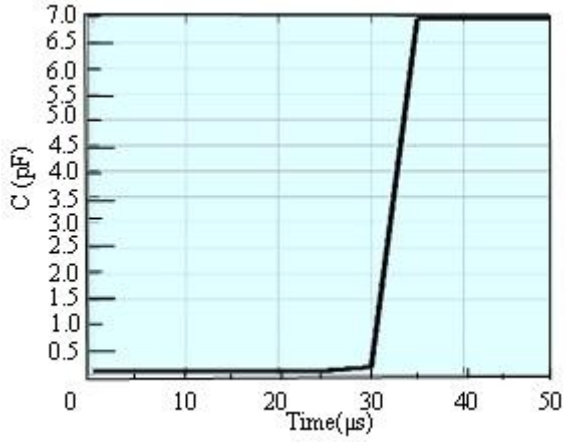

Figure 10. Capacitances of switch-on and switch-off.

5.3. RF Switch Parameters

The electromagnetic analysis of the optimized switch design was conducted using Advanced Design System (ADS) software. The index of dispersion, represented by the S parameters, was simulated. In Figure 11, with no electrical voltage applied to the switch and in the off state, the return loss is S_{11} = −11.74 dB at a frequency of 40 GHz. Moreover, upon applying the actuation voltage to the membrane surface and turning on the switch, the insertion loss is S_{21} = −34.62 dB at the frequency of 40 GHz, as depicted in Figure 12.

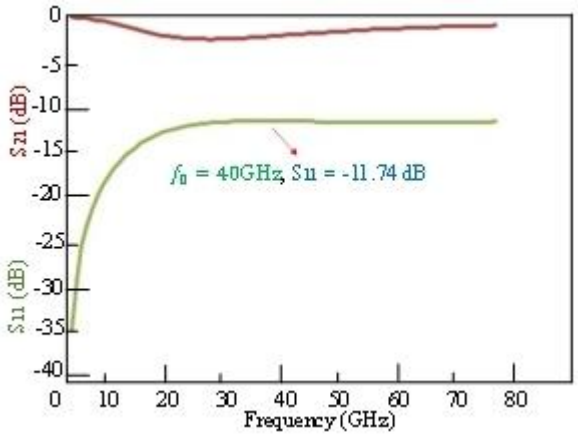

Figure 11. S-parameters of switch-up state.

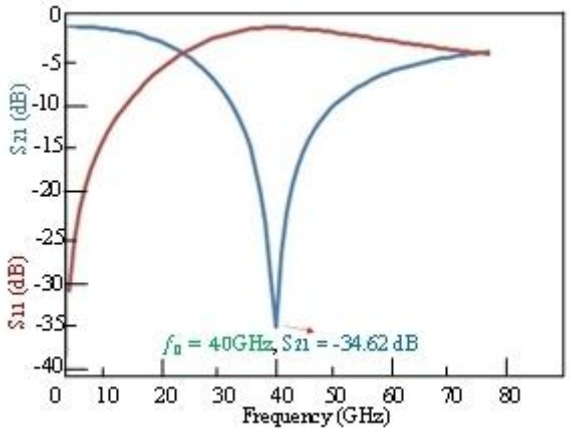

Figure 12. S-parameters of switch-down state.

6. Results and Conclusions

The study developed a multi-objective model to determine the actuation voltage, insertion loss in the up-state, and isolation in the down-state of an aluminum switch using mathematical programming. The proposed model was solved using the Multi-Objective Particle Swarm Optimization (MOPSO) meta-heuristic algorithm and the utility algorithm. Extracting the Pareto solution set allowed for determining the actuation voltage, insertion loss, and isolation, with a spring constant of k = 1.033 N/m achieved using five membranes in a flexure Serpentine configuration. Design parameters such as length (45), width (4.5), thickness (1.5), and the number of membranes (4) were selected to minimize the objective function of the switch. After optimizing the RF MEMS switch design, the electrostatic pull-in voltage was calculated as 2.8 V. The response time of the MEMS switch was approximately 15 µs, and the capacitance ratio was equal to 70. The return loss and insertion loss were determined as S_{11} = −11.74 dB and S_{21} = −34.62 dB, respectively, for the optimized switch at a frequency of 40 GHz. Table 6 presents a comparison of our work with some typical developed capacitive RF-MEMS switches. The designed switch demonstrates superior performance, with an optimal spring constant compared to previous works [9,13–15,18,30], along with lower actuation voltage, isolation, and insertion loss. These achievements

were realized through a balanced compromise between parameters. The design stands out for its remarkable performance and appropriateness compared to prior research, showcasing its effectiveness and efficiency in achieving optimal performance metrics in microelectromechanical systems. This paper introduces a pioneering strategy aimed at reducing the transient response time of a standalone micro pump switch. Notably, our discussion does not encompass the configuration of other sections of the micro pump, which could be explored in future research endeavors. Our findings validate that through the proposed approach, the transient response time of the switch diminishes concomitantly with a reduction in the actuation voltage.

Table 6. Comparison of developed capacitive RF-MEMES switches.

RF-MEMS Switch	[15]	[13]	[30]	[18]	[14]	[9]	DOE
Actuation Voltage	7 V	82 V	23.6 V	23.5 V	3 V	3.04 V	2.8 V
Spring Constant	0.27 N/m	-	1.43 N/m	-	0.65 N/m	1.3 N/m	1.13 N/m
Air Gap (g_{gap})	1.1 µm	-	3 µm	2.5 µm	2.2 µm	1.397 µm	1.4 µm
Dielectric	SiO, ε_r = 3.9	SiO, ε_r = 3.9	AIN, ε_r = 9.8	Si_3N_4, ε_r = 6–7	SiO_2, ε_r = 4.99	SiO_2, ε_r = 4.99	SiO_2, ε_r = 4.99
S_{11}	−3.1 dB	−0.9 dB	−0.68 dB	−0.8 dB	-	−5.6 dB	−11.74 dB
S_{21}	−15 dB	−17 dB	−35.7 dB	−60 dB	-	−24 dB	−34.62 dB
Actuation Time	8.2 µs	49 µs	8.2 µs	23 µs	-	30 µs	15 µs

Author Contributions

Conceptualization, A.A. and F.S.; methodology, A.A. and F.S.; validation, A.A; formal analysis, A.A.; data curation. F.S. and M.N.; writing—original draft preparation, A.A., and F.S.; writing—review and editing, A.A., F.S., M.M. and M.N.; visualization, A.A., F.S. and M.N. All authors have read and agreed to the published version of the manuscript.

Funding

This work received no external funding.

Institutional Review Board Statement

Not applicable.

Informed Consent Statement

Not applicable.

Conflicts of Interest

The authors declare no conflict of interest.

References

1. Joshitha, C.; Sreeja, B.S.; Radha, S. A Review on Micropumps for Drug Delivery System. In Proceedings of the 2017 International Conference on Wireless Communications, Signal Processing and Networking (WiSPNET), Chennai, India, 22–24 March 2017. [CrossRef]
2. Rebeiz, G.M.; Muldavin, J.B. RF MEMS Switches and Switch Circuits. *IEEE Microw. Mag.* **2001**, *2*, 59–71. [CrossRef]
3. Soltanian, F.; Baghelani, M. Fault Detection and Diagnosis of RF MEMS Resonators. In Proceedings of the First International Conference on MEMS and Microfabrication-ICMEMS2014, New Technologies Research Center, Amirkabir University of Technology, Tehran, Iran, 18–19 February 2014.

4. Cortes, V.S.; Fischer, G. Shunt MEMS Switch Requirements for Tunable Matching Network at 1.9 GHz in Composite Substrates.In Proceedings of the 2015 German Microwave Conference, Nuremberg, Germany, 16–18 March 2015. [CrossRef]
5. Guo, F.M.; Zhu, Z.Q.; Long, Y.F.; Wang, W.M.; Zhu, S.Z.; Lai, Z.S.; Li, N.; Yang, G.Q.; Lu, W. 2003. Study on Low Voltage Actuated MEMS RF Capacitive Switches. *Sensors Actuators, A Phys.* **2003**, *108*, 128–133. [CrossRef]
6. Liu, G.; Yang, F.; Bao, X.; Jiang, T. Robust Optimization of a MEMS Accelerometer Considering Temperature Variations. *Sensors (Switzerland)* **2015**, *15*, 6342–6359. [CrossRef]
7. Ma, L.Y.; Nordin, A.N.; Soin, N. Design, Optimization and Simulation of a Low-voltage Shunt Capacitive RF-MEMS Switch. *Microsyst. Technol.* **2016**, *22,* 537–549. [CrossRef]
8. Shekhar, S.; Vinoy, K.J.; Ananthasuresh, G.K. Surface-Micromachined Capacitive RF Switches with Low Actuation Voltage and Steady Contact. *Microsyst. Technol.* **2018**, *26*, 643–652. [CrossRef]
9. Deng, Z.; Wei, H.; Fan, S.;. Gan, J. Design and Analysis a Novel RF MEMS Switched Capacitor for Low Pull—in Voltage Application. *Microsyst. Technol.* **2015**, *22*, 2141–2149. [CrossRef]
10. Sravani, K.G.; Narayana, T.L.; Guha, K.; Rao, K.S. Role of Dielectric and Different Membrane Thin Films in Improving the Performance Of Capacitive Mems Switches Over Ka-Band Applications Role of Dielectric Layer and Beam Membrane in Improving the Performance of Capacitive Rf Mems Switches For Ka-Band Appl. *Microsyst. Technol.* **2018**, *27*, 493–502. [CrossRef]
11. Molaei, S.; Ganji, B.A. Design and Simulation of a Novel Rf Mems Shunt Capacitive Switch with Low Actuation Voltage and High Isolation. *Microsyst. Technol.* **2017**, 23, 1907–1912. [CrossRef]
12. Ya, M.L.; Nordin, A.N.; Soin, N. Design and Analysis of a Low-Voltage Electrostatic Actuated RF CMOS-MEMS Switch. In Proceedings of the RSM 2013 IEEE Regional Symposium on Micro and Nanoelectronics, Daerah Langkawi, 25–27 September 2013. [CrossRef]
13. Bartolucci, G.; De Angelis, G.; Lucibello, A.; Marcelli, R.; Proietti, E. Analytic Modeling of RF MEMS Shunt Connected Capacitive Switches. *J. Electromagn. Waves Appl.* **2012**, *26*, 1168–1179. [CrossRef]
14. Chircov, C.; Grumezescu, A.M. Microelectromechanical Systems (MEMS) for Biomedical Applications. *Micromachines* **2022**, 13, 164. [CrossRef]
15. Bußmann, A.B.; Grünerbel, L.M.; Durasiewicz, C.P.; Thalhofer, T.A.; Wille, A.; Richter, M. Microdosing for Drug Delivery Application—A Review. *Sens. Actuators, A: Phys.* **2021**, *330*, 112820. [CrossRef]
16. Chappel, E.; Dumont-Fillon, D. Chapter 3—Micropumps for Drug Delivery. *Drug Delivery Devices Ther. Syst.* **2021**, 31–61. [CrossRef]
17. Coln, E.A.; Colon, A.; Long, C.J.; Sriram, N.N.; Esch, M.; Prot, J.; Elbrecht, D.H.; Wang, Y.; Jackson, M; Hickman, J.J.; Shuler, M.L. Piezoelectric BioMEMS Cantilever for Measurement of Muscle Contraction and for Actuation of Mechanosensitive Cells. *MRS Commun.* **2019**, 9, 1186–1192. [CrossRef]
18. Kumar, P.A.; Sravani, K.G.; Sailaja, B.V.S.; Vineetha, K.V.; Guha, K.; Rao, K.S. Performance Analysis of Series: Shunt Configuration-Based RF MEMS Switch for Satellite Communication Applications. *Microsyst Technol.* **2018**, *24,* 4909–4920. [CrossRef]
19. Maluf, N.; Williams, K. An introduction to microelectromechanical systems engineering. Artech House; 2004. Available online: https://us.artechhouse.com/mobile/An-Introduction-to-Microelectromechanical-Systems-Engineering-Second-Edition-P806.aspx?gad_source=1&gclid=EAIaIQobChMI6Juizu-bhgMVJhB7Bx24-gy-EAAYAiAAEgJcN_D_BwE (accessed on 23 September 2023)
20. Rebeiz, G.M. *RF MEMS: Theory, Design and Technology*. John Wiley & Sons, Inc.: New Jersey, USA, 2003; pp. 87–121. [CrossRef]
21. Rabinovich, V.L.; Gupta, R.K.; Senturia, S.D. The Effect of Release-etch Holes on the Electromechanical Behaviour of MEMS Structures. In Proceedings of International Solid State Sensors and Actuators Conference (Transducers '97), Chicago, USA, 19 June 1997. [CrossRef]
22. Peroulis, D.; Pacheco, S.P.; Sarabandi, K.; Katehi, L.P.B. Electromechanical Considerations in Developing Low-voltage RF MEMS Switches. *IEEE Trans. Microw. Theory Tech.* **2003**, *51*, 259–270. [CrossRef]
23. Singh, T. Design and Finite Element Modeling of Series-shunt Configuration-based RF MEMS Switch for High Isolation Operation in K-Ka Band. *J. Comput. Electron.* **2014**, *14*, 167–179. [CrossRef]
24. Bazaraa M.S.; Jarvis J.J.; Sherali, H.D. *Linear Programming and Network Flows*, John Wiley & Sons, Inc.: New Jersey, USA, 2009. [CrossRef]
25. Fan, Z.; Seo, K.; Hu, J.; Goodman, E.D.; Rosenberg, R.C. A Novel Evolutionary Engineering Design Approach for Mixed-Domain Systems. *Eng. Optim.* **2004**, *36*, 127–147. [CrossRef]
26. Abraham, A.S.K. Patterns of Landholding and Architectural Patronage in Late Medieval Meath: A Regional Study of the Landholding Classes, tower Houses and Parish Churches in Ireland, c. 1300-c. 1540. (1995): 0026-0026. Available online: https://www.elibrary.ru/query_results.asp (accessed on 23 September 2023).

27. Ranginkaman, M.H.; Haghighi, A.; Samani, H.M.V. Inverse Frequency Response Analysis for Pipelines Leak Detection Using the Particle Swarm Optimization. *Int. J. Optim. Civ. Eng.* **2016**, *6*, 1–12. [CrossRef]
28. Noorollahi, E.; Fadai, D.; Ghodsipour, S.H.; Shirazi, M.A. Developing a New Optimization Framework for Power Generation Expansion Planning with the Inclusion of Renewable Energy - A Case Study of Iran. *J. Renew. Sustain. Energy* **2017**, *9*, 015901. [CrossRef]
29. Jaafar, H.; Beh, K.S.; Yunus, N.A.M.; Hasan, W.Z.W.; Shafie, S.; Sidek, O. A Comprehensive Study on RF MEMS Switch. *Microsyst. Techno*l. **2014**, *20*, 2109–2121. [CrossRef]
30. Angira, M.; Sundaram, G.M.; Rangra, K.J. A Novel Approach for Low Insertion Loss, Multi-band, Capacitive Shunt RF–MEMS Switch. *Wirel. Pers. Commun.* **2015**, *83*, 2289–2301. [CrossRef]